AIAA SciTech Forum
7-11 January 2019, San Diego, California
AIAA Scitech 2019 Forum

10.2514/6.2019-0034

Study of 3D Co-flow Jet Wing Induced Drag and Power Consumption at Cruise Conditions

Yang Wang * Gecheng Zha †
Dept. of Mechanical and Aerospace Engineering
University of Miami, Coral Gables, Florida 33124
E-mail: gzha@miami.edu

Abstract

This paper presents the study of induced drag of 3D Co-Flow Jet (CFJ) wing at cruise conditions with different aspect ratios. The simulated aspect ratios are 20, 10 and 5. The wings are formed by two CFJ airfoils, namely CFJ 1 and CFJ 2, both modified from NACA 6421 airfoil with the injection slot size and suction slot size of the CFJ 2 enlarged by 80% and 85% respectively compared with the CFJ 1. The baseline wings with the non-controlled NACA 6421 airfoil are also simulated for comparison at the same aspect ratios. A momentum coefficient C_μ of 0.03 and 0.04 are used at the cruise condition with optimum aerodynamic efficiency and productivity efficiency. The angle of attack (AoA) is fixed at 5°, which produces the optimum aerodynamic for the two CFJ wings and the baseline wings. The simulations employ the validated in house FASIP CFD code, utilizing a 3D RANS solver with Spalart-Allmaras (S-A) turbulence model, 3rd order WENO scheme for the inviscid fluxes, and 2nd order central differencing for the viscous terms.

The study indicates that the induced drag coefficient of CFJ wings is increased with the decrease of aspect ratio. However, the Oswald efficiency is also increased with decreasing aspect ratio. The CFJ wings have higher Oswald efficiency than the baseline wings with the same aspect ratio becasue the lift enhancement effect outperforms the induced drag increase. In other words, the CFJ wing is less penalized even though the lift coefficient is higher than the baseline wing. The CFJ wing always has substantially higher ratio of C_L/C_D than the baseline wing since CFJ reduces the pressure drag significantly. For the corrected aerodynamic efficiency of $(C_L/C_D)_c$ that includes the CFJ power consumption, the CFJ 2 wing's result is slightly better than the baseline wing at aspect ratio of 20 and similar at aspect ratio of 10 and 5. However, attributed to the increased cruise lift coefficient, the productivity efficiency of the CFJ 2 wing measured by $(C_L^2/C_D)_c$ is increased by 32.1% for the wing of AR 20, 19.4% for AR 10 and 5.6% for AR 5.

For the power consumption comparison, the CFJ 2 wings at all aspect ratios have substantially lower CFJ power coefficient benefited from the larger injection and suction slot size. For the same momentum coefficient, the CFJ 2 wings with larger slot size have lower injection velocity, lower total pressure ratio between the injection and suction slot, and larger mass flow rate. The CFJ power coefficient is determined linearly by the mass flow rate, but exponentially by the total pressure ratio. Hence a decrease of the total pressure ratio has the major impact to reduce the CFJ power consumption. As a result, the productivity efficiency of the CFJ 2 wing is increased by 12.9%, 9.8% and 8.7% for AR 20, 10 and 5 respectively compared with the CFJ 1 wing.

In conclusion, the CFJ wing is much more efficient than the baseline wing at either high or low aspect ratio. Furthermore, the CFJ power consumption can be substantially reduced by using large slot size with reduced injection jet velocity and jet total pressure ratio. This is particularly important for the same CFJ airfoil with fixed geometry to be used for whole flight envelop from takeoff to cruise and landing.

* Graduate Student
† Professor, AIAA associate Fellow

Nomenclature

CFJ	Co-flow jet
AoA	Angle of attack
LE	Leading Edge
TE	Trailing Edge
S	Planform area
s	Wing Span length
c	Profile chord
U	Flow velocity
q	Dynamic pressure $0.5\,\rho\,U^2$
p	Static pressure
ρ	Air density
$\dot{m}$	Mass flow
M	Mach number
ω	Pitching Moment
P	Pumping power
∞	Free stream conditions
$_j$	Jet conditions
C_L	Lift coefficient $L/(q_\infty\,S)$
C_D	Drag coefficient $D/(q_\infty\,S)$
C_M	Moment coefficient $M/(q_\infty\,S)$
C_μ	Jet momentum coefficient $\dot{m}_j\,U_j/(q_\infty\,S)$
$(C_L/C_D)_c$	CFJ airfoil corrected efficiency $C_L/(C_D+\,P/V_\infty)$
$(C_L^2/C_D)_c$	CFJ airfoil productivity efficiency $C_L^2/(C_D+\,P/V_\infty)$
P_c	Power coefficient $P/(0.5\,\rho_\infty\,V_\infty^3\,S)$
e	Oswald efficiency
V_{inj}/V_∞	Normalized injection velocity
C_{Di}	Induced drag coefficient
C_{Dc}	Drag coefficient plus its Power coefficient for CFJ airfoil
C_{D0}	Drag coefficient at zero lift angle of attack
M_{is}	Isentropic Mach Number
P_{tinj}	Total injection pressure
P_{tsuc}	Total suction pressure
PR	Total Pressure ratio of the CFJ pump

1 Introduction

Recently, Co-Flow Jet (CFJ) flow control airfoil developed by Zha et al. [1, 2, 3, 4, 5, 6, 7, 8, 9, 10, 11, 12, 13] is demonstrated to achieve radical lift augmentation, stall margin increase, drag reduction and nose-down moment increase for stationary and pitching airfoils. In a CFJ airfoil, an injection slot near the leading edge (LE) and a suction slot near the trailing edge (TE) on the airfoil suction surface are created. As shown in Fig. 1, a small amount of mass flow is drawn into the suction duct, pressurized and energized by the micro compressor, and then injected near the LE tangentially to the main flow via an injection duct. The whole process does not add any mass flow to the system and hence is a zero-net-mass-flux(ZNMF) flow control.

A full electric 4-seats long range and compact CFJ airplane is first designed by Lefebvre and Zha[14] and demonstrates a substantial range increase compared with the same size aircraft with conventional design. Yang and Zha [15] further improve the productivity efficiency significantly. A fixed aspect ratio of 20 is used in the designs[14, 15] and no study on the induced drag is conducted. Even though the 3D CFJ wing performance is studied by Lefebvre and Zha[12], the focus is on the overall performance of cruise and takeoff/landing. Since CFJ wings typically fly at substantially higher lift coefficient either at cruise or takeoff/landing, a question that needs to be answered is how the induced drag due to lift behaves. The induced drag is important to determine the efficiency of all aircraft design. The second question is how to reduce the CFJ power consumption and still keep the same lift coefficient in order to maximize the cruise efficiency. The purpose of this paper is to study these two problems by simulating 3D CFJ wings with different aspect ratios and different slots sizes, but with a constant jet injection momentum coefficient at a fixed optimum cruise angle of attack.

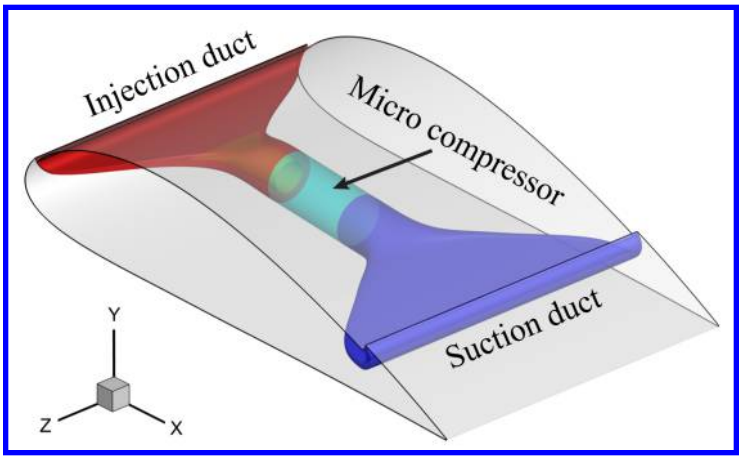

Figure 1: Schematic plot of a typical CFJ airfoil.

2 Methodology

2.1 Lift and Drag Calculation

The momentum and pressure at the injection and suction slots produce a reactionary force, which is automatically measured by the force balance in wind tunnel testing. However, for CFD simulation, the full reactionary force needs to be included. Using control volume analysis, the reactionary force can be calculated using the flow parameters at the injection and suction slot opening surfaces. Zha et al. [2] give the following formulations to calculate the lift and drag due to the jet reactionary force for a CFJ airfoil. By considering the effects of injection and suction jets on the CFJ airfoil, the expressions for these reactionary forces are given as :

$$F_{x_{cfj}} = (\dot{m}_j V_{j1} + p_{j1} A_{j1}) * cos(\theta_1 - \alpha) - (\dot{m}_j V_{j2} + p_{j2} A_{j2}) * cos(\theta_2 + \alpha) \tag{1}$$

$$F_{y_{cfj}} = (\dot{m}_{j1} V_{j1} + p_{j1} A_{j1}) * sin(\theta_1 - \alpha) + (\dot{m}_{j2} V_{j2} + p_{j2} A_{j2}) * sin(\theta_2 + \alpha) \tag{2}$$

where the subscripts 1 and 2 stand for the injection and suction respectively, and θ_1 and θ_2 are the angles between the injection and suction slot's surface and a line normal to the airfoil chord. α is the angle of attack.

The total lift and drag on the airfoil can then be expressed as:

$$D = R'_x - F_{x_{cfj}} \tag{3}$$

$$L = R'_y - F_{y_{cfj}} \tag{4}$$

where R'_x and R'_y are the surface integral of pressure and shear stress in x (drag) and y (lift) direction excluding the internal ducts of injection and suction. For CFJ wing simulations, the total lift and drag are calculated by integrating Eqs.(3) and (4) in the spanwise direction.

2.2 Jet Momentum Coefficient

The jet momentum coefficient C_μ is a parameter used to quantify the jet intensity. It is defined as:

$$C_\mu = \frac{\dot{m} V_j}{\frac{1}{2}\rho_\infty {V_\infty}^2 S} \tag{5}$$

where $\dot{m}$ is the injection mass flow, V_j is the mass-averaged injection velocity, ρ_∞ and V_∞ denote the free stream density and velocity, and S is the planform area.

2.3 Power Coefficient

CFJ is implemented by mounting a micro-compressor system inside the wing that withdraws air from the suction slot and blows it into the injection slot. The power consumption is determined by the jet mass flow and total enthalpy change as the following:

$$P = \dot{m}(H_{t1} - H_{t2}) \tag{6}$$

where H_{t1} and H_{t2} are the mass-averaged total enthalpy in the injection cavity and suction cavity respectively, P is the Power required by the pump and $\dot{m}$ the jet mass flow rate. Introducing P_{t1} and P_{t2} the mass-averaged total pressure in the injection and suction cavity respectively, the pump efficiency η, and the total pressure ratio of the pump $\Gamma = \frac{P_{t1}}{P_{t2}}$, the power consumption is expressed as:

$$P = \frac{\dot{m} C_p T_{t2}}{\eta}(\Gamma^{\frac{\gamma-1}{\gamma}} - 1) \tag{7}$$

where γ is the specific heat ratio equal to 1.4 for air. The power coefficient is expressed as:

$$P_c = \frac{P}{\frac{1}{2}\rho_\infty V_\infty^3 S} \tag{8}$$

2.4 Corrected Aerodynamic Efficiency

The conventional wing aerodynamic efficiency is defined as:

$$\frac{L}{D} \tag{9}$$

For the CFJ wing, the ratio above still represents the pure aerodynamic relationship between lift and drag. However since CFJ active flow control consumes energy, the ratio above is modified to take into account the energy consumption of the pump. The formulation of the corrected aerodynamic efficiency for CFJ wings is:

$$(\frac{L}{D})_c = \frac{C_L}{C_D + P_c} \tag{10}$$

where V_∞ is the free stream velocity, P is the pumping power, and L and D are the lift and drag generated by the CFJ wing. The formulation above converts the power consumed by the CFJ into a force $\frac{P}{V_\infty}$ which is added to the aerodynamic drag D. If the pumping power is set to 0, this formulation returns to the aerodynamic efficiency of a conventional wing.

2.5 Aircraft Productivity

To compare aircraft that have the same ratio of initial weight to final weight with the same engine fuel consumption or battery energy density, the productivity efficiency C_L^2/C_D is introduced to measure the productivity of an airplane represented by its range multiplied by its weight [16].

The productivity efficiency $C_L^2/C_D = C_L(C_L/C_D)$ is a more comprehensive parameter than the conventional aerodynamic efficiency C_L/C_D to measure the merit of an airplane aerodynamic design for cruise performance. The former includes not only the information of C_L/C_D, but also the information of the aircraft weight C_L. For example, for two airplane designs having the same C_L/C_D with one C_L twice larger than the other, if the wing sizes are the same, one airplane will be able to carry twice more weight than the other with productivity and wing loading increased by 100%. Such a large difference is not reflected by C_L/C_D, but very well reflected by C_L^2/C_D.

The definition of C_L/C_D in general is a suitable measure of merit for conventional aircraft design. This is because at a certain Mach number regime, the maximum C_L/C_D is usually achieved at low angle of attack within the drag bucket and is more or less the same for different airfoil designs. In other words, for the same optimum C_L/C_D, the C_L is about the same. A typical C_L for subsonic airfoil is about 0.4 - 0.5 and for transonic airfoil is about 0.7.

For CFJ airfoil, the minimum CFJ pumping power occurs at a fairly high AoA [7, 17]. With the augmentation of CFJ, the subsonic cruise lift coefficient of a CFJ airfoil is typically 2 to 3 times higher than the conventional airfoil with about the same $(C_L/C_D)_c$ [12]. Such a high lift coefficient is unattainable for conventional airfoil since they would be either stalled or near stalled with very high drag. Hence for CFJ aircraft design, the productivity efficiency $C_L^2/C_D = C_L(C_L/C_D)$ is more informative to be used to reflect the aerodynamic performance. The corrected productivity efficiency for CFJ airfoils is $(C_L^2/C_D)_c = C_L^2/(C_D + P_c)$.

2.6 Oswald Efficiency

The Oswald efficiency is a correction factor that represents induced drag effect when a 3D wing platform is deviated from an elliptic platform. The total drag coefficient of an airplane can be expressed as:

$$C_D = C_{D0} + C_{Di} \tag{11}$$

$$C_{Di} = C_D - C_{D0} = \frac{C_L^2}{\pi e AR} \tag{12}$$

where C_{Di} is the induced drag coefficient, e is the Oswald efficiency, AR is the aspect ratio, C_{D0} is the zero-lift drag coefficient, C_L is the total lift coefficient, and C_D is the total drag coefficient. Using the formulation above, we can calculate the Oswald efficiency with the known values of C_L, C_D, AR, and C_{D0} as below:

$$e = \frac{C_L^2}{\pi C_{Di} AR} \tag{13}$$

2.7 CFD Simulation Setup

The in house FASIP (Flow-Acoustics-Structure Interaction Package) CFD code is used to conduct the numerical simulation. The 3D Reynolds Averaged Navier-Stokes (RANS) equations with one-equation Spalart-Allmaras [18] turbulence model is used. A 3rd order WENO scheme for the inviscid flux [19, 20, 21, 22, 23, 24] and a 2nd order central differencing for the viscous terms [19, 23] are employed to discretize the Navier-Stokes equations. The low diffusion E-CUSP scheme used as the approximate Riemann solver suggested by Zha et al [20] is utilized with the WENO scheme to evaluate the inviscid fluxes. Implicit time marching method using Gauss-Seidel line relaxation is used to achieve a fast convergence rate [25]. Parallel computing is implemented to save wall clock simulation time [26].

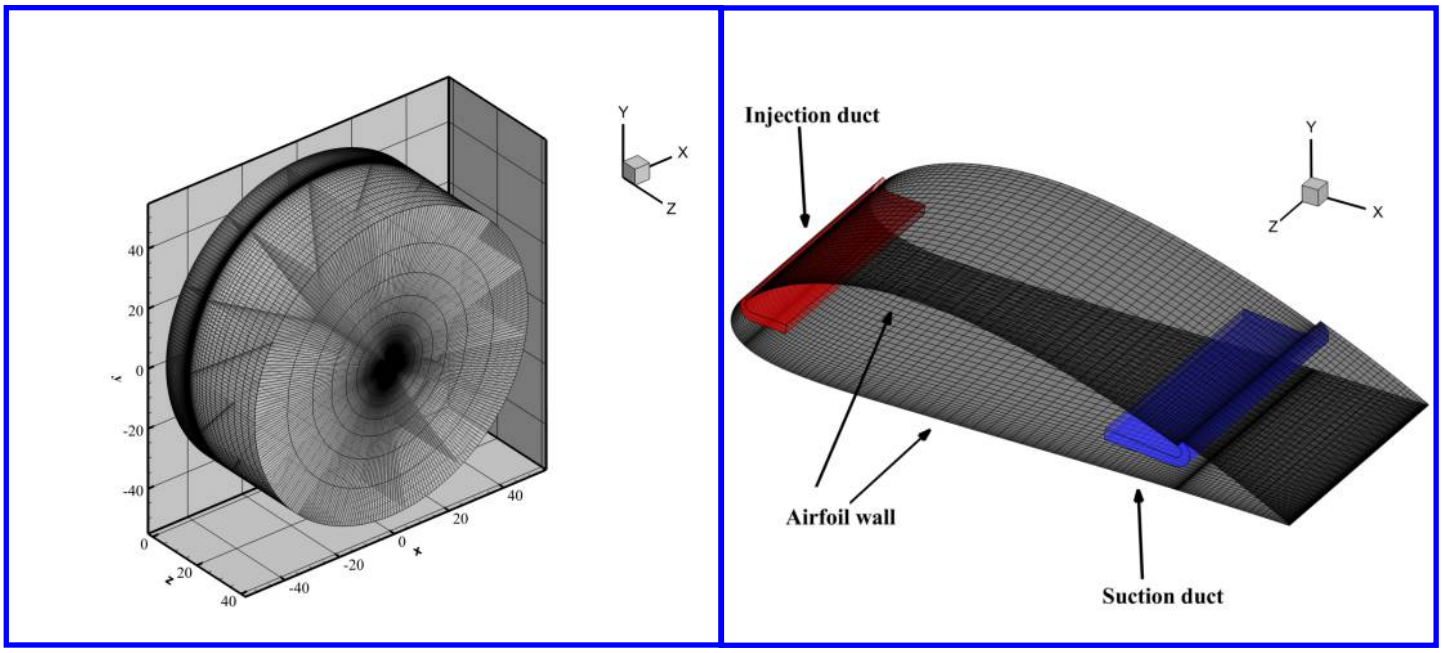

(a) (b)

Figure 2: Computational mesh used in the current work.

2.8 Boundary Conditions

The 3rd order accuracy no slip condition is enforced on the solid surface with the wall treatment suggested in [27] to achieve the flux conservation on the wall. The computational mesh is shown in Fig. 2 with O-mesh topology and the radial farfield boundary located at 20 chord radius. The spanwise farfield is located at 20 chord away from the wing tip. Total pressure, total temperature and flow angles are specified at the injection duct inlet, as well as the upstream portion of the far field. Constant static pressure is applied at the suction duct outlet as well as the downstream portion of the far field. Symmetry boundary conditions are applied at the root of the wing, whereas the wing tip flow is resolved by a mesh block. The cross-section faces of the CFJ ducts are meshed using "H" topology while the domains around the airfoil are meshed using "O" topology. The total mesh size is 3.918 millions points, split into 111 blocks for the parallel computation. The first grid point on the wing surface is placed at $y^+ \approx 1$. This mesh size is the same as the one used in the study of Lefebvre and Zha[12], which the mesh is verified for mesh independence.

3 Results and Discussion

In this section, we present the results of two designs of CFJ wings and baseline wings at different aspect ratio. The CFJ 1 wing is the one previously designed by Lefebvre and Zha[12], which is modified from the NACA 6421 airfoil with the suction surface translated downward by 1.5% Chord. The CFJ 2 is the optimized wing based on the CFJ 1 with enlarged injection and suction slot by 80% and 85% respectively. The baseline wing uses the NACA 6421 airfoil with no CFJ. The simulation parameters are listed in Table 1, which indicates that the aspect ratio studied are 20, 10, and 5. The CFJ 2 wing is simulated at C_μ of 0.03 and 0.04. For the CFJ 1 wing, only C_μ of 0.04 is simulated.

Table 1: 3D Wings simulated.

Cases	AR	Mach	AoA	C_μ	Airfoil
CFJ 1	20, 10, 5	0.15	5°	0.03	CFJ6421-SST150-SUC133-INJ065
CFJ 2	20, 10, 5	0.15	5°	0.03, 0.04	CFJ6421-SST150-SUC247-INJ117
Baseline	20, 10, 5	0.15	5°	N/A	Baseline NACA 6421

Table 2 gives the detailed geometric parameters of the two different designs of CFJ-NACA-6421 airfoils with the injection and suction slot size normalized by airfoil chord length (C). The CFJ 1 wing has an injection slot size of 0.65%C and suction slot size of 1.33%C, and the suction surface translation (SST) of 1.50%C. The CFJ 2 wing has the same SST, but an 80% larger injection slot size of 1.17%C and an 85% larger suction slot size of 2.47%C.

Table 2: Airfoil geometry parameters.

Airfoil	SST (%C)	INJ slot size (%C)	SUC slot size (%C)
3D CFJ 1	1.50	0.65	1.33
3D CFJ 2	1.50	1.17	2.47

Since the interest of this paper is on cruise performance, the AoA rang studied is at the low level from $-10°$ to $15°$ with a $5°$ step size. Among those angle of attack, AoA of $5°$ always gives the optimum corrected aerodynamic efficiency for both the baseline wings and CFJ wings. Thus, all the results comparison below are presented at AoA of $5°$ only.

As shown in Fig. 3(a), the C_L is increased with the increase of aspect ratio since a higher aspect ratio is closer to 2D airfoil with less tip vortex and down-wash effect. At the same jet momentum of 0.04, the CFJ 1 wing and CFJ 2 wing have about the same C_L at the same aspect ratio. Lowering the jet momentum to 0.03 slightly decreases the enhancement of the C_L. The CFJ wing always has a substantially higher cruise lift coefficient than the baseline wing.

Fig. 3(b) shows that with the increasing of aspect ratio, the drag coefficient of the CFJ wings is largely decreased and become lower than that of the baseline at AR 20. The C_D for CFJ 1 wing and CFJ 2 wing are similar at C_μ of 0.04, the reduction of C_μ to 0.03 slightly increase the C_D at low aspect ratio, but have about the same C_D at aspect ratio of 20.

Fig. 3(c) shows that the CFJ wings have substantially higher value of the nose-down moment than the baseline wing. However, the CFJ 2 wing has smaller nose down moment value than the CFJ 1 even though they have about the same lift coefficient. The smaller C_μ generates about the same pitching moment. A tandem wing or a canard configuration with the front wing used to balance the nose down moment is hence desirable. The pitching moment coefficient of the baseline wing almost remains the same at all aspect ratio.

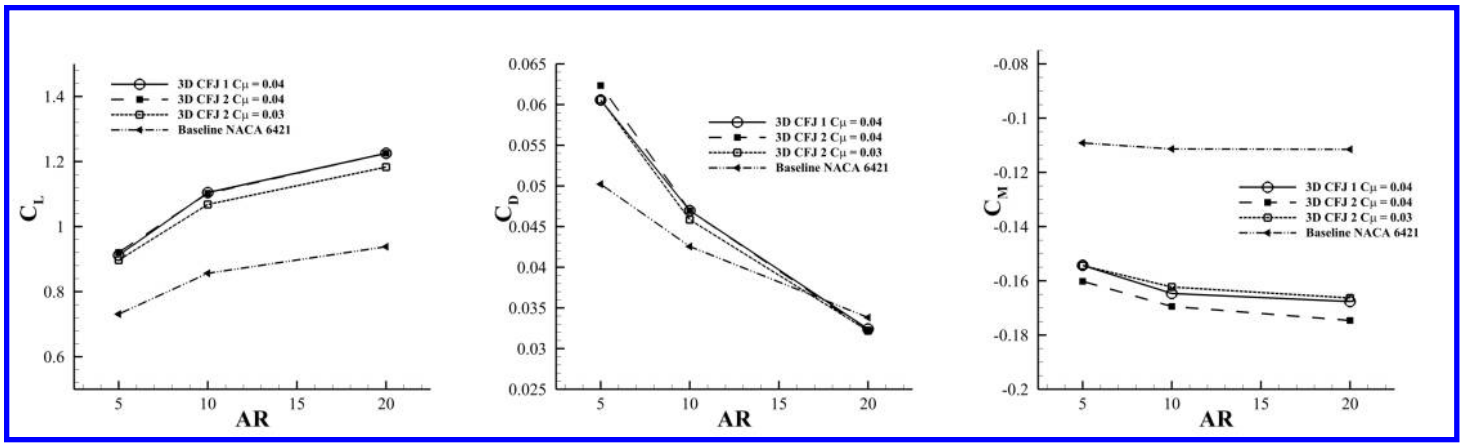

(a) (b) (c)

Figure 3: Lift, drag and moment coefficients for the CFJ 1 wing, the CFJ 2 wing and baseline wing.

The C_L/C_D, $(C_L/C_D)_c$, $(C_L{}^2/C_D)_c$ plots for both CFJ wings and baseline wings are shown in Fig. 4. As shown in Fig. 4(b), for the AR of 5, the CFJ wing and the baseline wing have about the same C_L/C_D, but the C_L level of CFJ wing is substantially higher than that of the baseline as shown in Fig. 3(a). With the AR increased to 20, the C_L/C_D is also increased to about 38% higher since the CFJ reduces the pressure drag significantly. For the corrected aerodynamic efficiency of $(C_L/C_D)_c$ that includes the CFJ power consumption (Fig.4(b)), the baseline wing has a higher $(C_L/C_D)_c$ at low AR of 5. When the AR is increased to 20, the CFJ 2 wing has about the same or slightly higher $(C_L/C_D)_c$ than the baseline wing. Although the corrected aerodynamic efficiencies are similar, the productivity efficiency of CFJ 2 wing at C_μ of 0.03 is increased by 32.1%, 19.4%, and 8.7% respectively for AR 20, 10, and 5 as shown in Fig.4(c) due to the higher cruise lift coefficient.

Fig. 5(a) compares the CFJ power coefficient. For the same C_μ of 0.04, the CFJ 2 wing substantially decreases the power coefficient by 30% with the same lift and drag coefficient as shown in Fig. 3. The reduced power coefficient contributes to the increase of aerodynamic efficiency and productivity efficiency demonstrated in Fig. 4. Such benefit is obtained completely by enlarging the injection and suction slot size. The power coefficient of CFJ 2 wing is further reduced by 35% when the C_μ is decreased from 0.04 to 0.03. A low cruise power requirement is crucial to achieve a high overall mission efficiency.

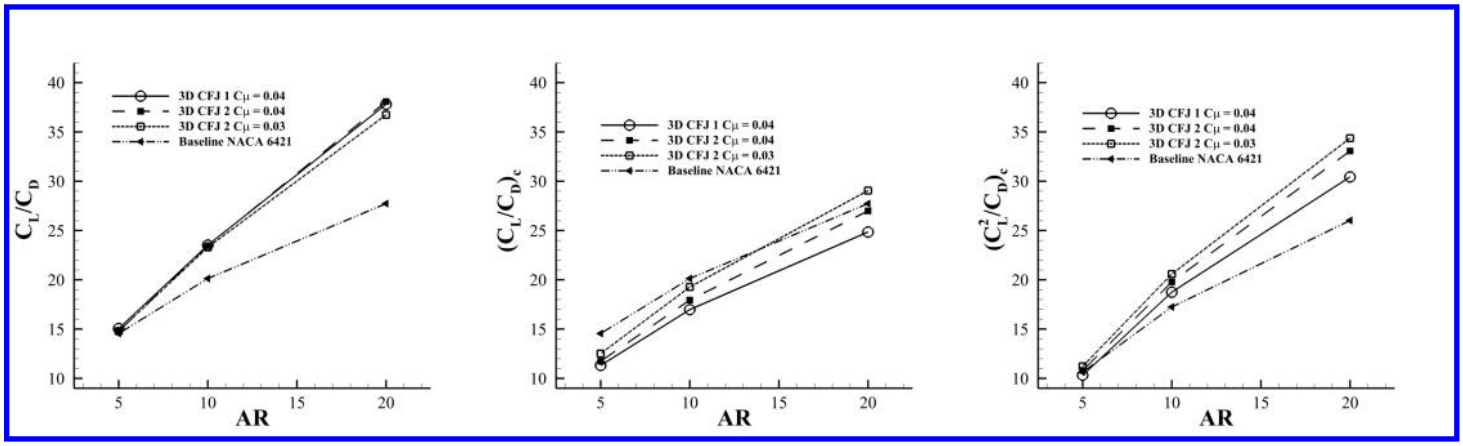

(a) (b) (c)

Figure 4: C_L/C_D, $(C_L/C_D)_c$, $(C_L{}^2/C_D)_c$ plots for the CFJ 1 wing, the CFJ 2 wing and baseline wing.

In order to calculate the Oswald efficiencies, the zero lift angle of attack needs to be found, so that the C_{D0} and C_{Di} in Eq. 11 and Eq. 12 can be determined. Table. 3 shows the zero lift AoA and the C_L and C_D values for all the two CFJ wings and the baseline wing. Note the C_L is only approximately equal to zero. For the CFJ wing, the zero lift occurs at about AoA of $-7°$. For the baseline wing, it is at about AoA of $-5.5°$. Also, the zero lift angle of attack decreases slightly for all the wings as the AR is decreased.

Table 3: C_L and C_D for Zero Lift AoA at different AR for all wings.

Airfoil	C_μ	AR	AoA(°)	C_L	C_D
3D CFJ 1	0.04	20	-7.29	0.00802	0.00549
3D CFJ 1	0.04	10	-7.33	0.00835	0.00638
3D CFJ 1	0.04	5	-7.40	0.00079	0.00799
3D CFJ 2	0.04	20	-6.91	0.00208	0.00915
3D CFJ 2	0.04	10	-7.01	-0.00486	0.00979
3D CFJ 2	0.04	5	-7.21	-0.01335	0.01182
Baseline	N/A	20	-5.56	-0.00097	0.01410
Baseline	N/A	10	-5.62	-0.00089	0.01471
Baseline	N/A	5	-5.72	-0.00102	0.01592

As shown in Fig. 5(b), a higher aspect ratio gives smaller induced drag coefficient at the same AoA. The CFJ wings also have higher induced drag coefficient than the baseline wings due to high lift coefficient. However, the CFJ wings all have higher Oswald efficiency than the baseline wings. Note that the Oswald efficiency is actually greater than 1 for the CFJ wings, indicating that the Oswald efficiency of a CFJ wing would be greater than that of an elliptic planform. The reason of the high Oswald efficiency is that the lift enhancement with the effect of exponential square term outperforms the increase of the induced drag coefficient as indicated by Eq. (13). This result means that the CFJ wing is penalized less than the baseline wing by the drag due to lift. This is also the reason that the CFJ wing achieves similar $(C_L/C_D)_c$ to the baseline wing (Fig. 4(b)), but at a substantially higher level of C_L, which produces much higher productivity efficiency as shown in Fig. 4(c). Fig. 5(c) indicates that the wing with AR of 5 gives higher Oswald efficiency than the wings of AR of 10 and 20 for both the CFJ and baseline wing.

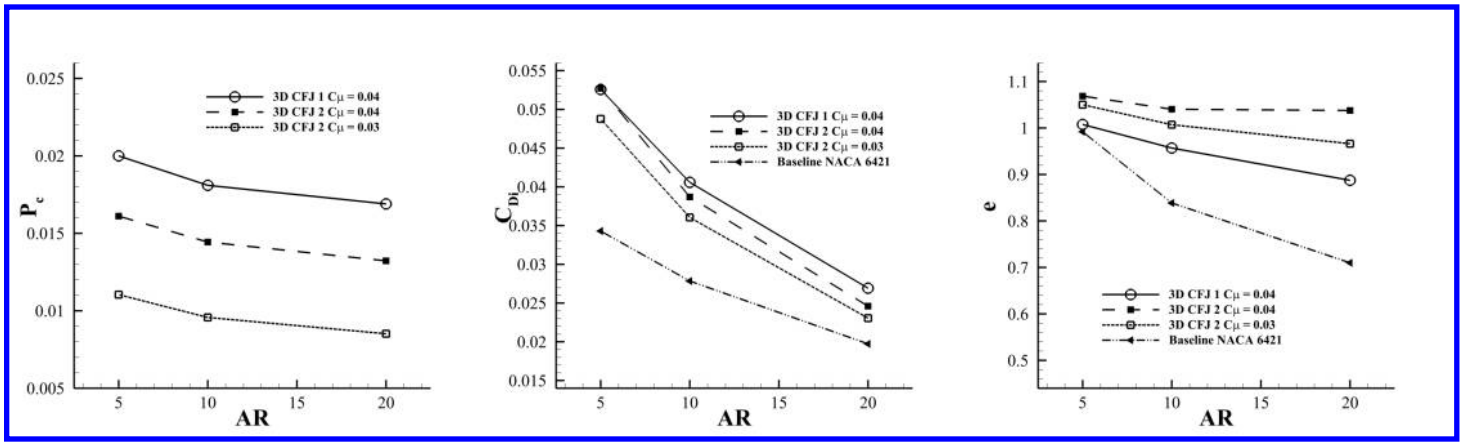

(a) (b) (c)

Figure 5: P_c, C_{Di}, Oswald efficiency e plots for the CFJ 1 wing, the CFJ 2 wing and baseline wing.

Fig. 6(a) shows the variation with the aspect ratio for Mass-averaged total pressure ratio (PR) between the injection and suction cavities, injection mass flow rate and normalized injection jet velocity for CFJ 1 and CFJ 2 wing. Fig.6(a) shows that the PR decreases slightly with the increase of aspect ratio due to the reduced loss caused by the tip vortex. For the same C_μ of 0.04, the CFJ 2 wing has substantially lower total pressure ratio than the CFJ 1 wing. The low total pressure ratio results in about 24% lower jet velocity as shown in Fig. 6(c). At the same time, the 80% enlarged injection slot area allows it to pass more mass flow rate as shown in Fig. 6(b). CFJ 2 wing achieves the same C_μ of 0.04 by using substantially lower injection velocity and high mass flow rate than the CFJ 1 wing. It benefits the CFJ 2 system with significantly lower total pressure, and most importantly lower power coefficient as shown in Fig. 5(a). This can be understood by analyzing Eq. (7), which indicates that the power coefficient is linearly determined by the CFJ mass flow rate and exponentially determined by the total pressure ratio between the injection slot and suction slot. The CFJ 2 wing consumes much lower power than the CFJ 1 wing for the same C_μ, lift augment and drag reduction because it has larger slot areas, lower injection jet velocity, lower total pressure ratio, and higher jet mass flow rate. The total pressure ratio dominates the power coefficient.

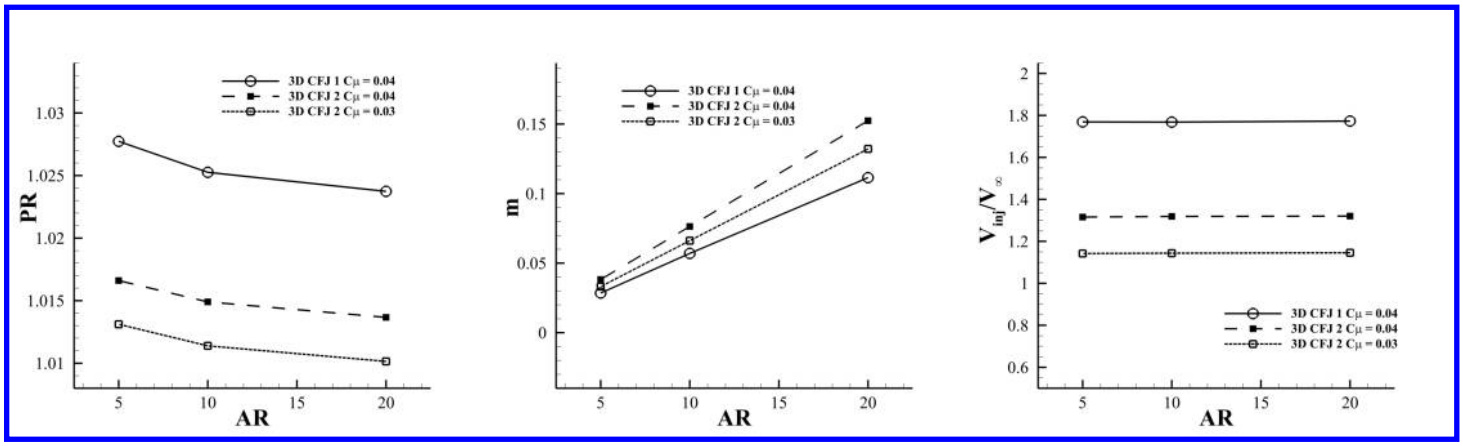

(a) (b) (c)

Figure 6: CFJ total pressure ratio, mass flow rate, and injection velocity variation with the aspect ratio.

The surface Isentropic Mach number (M_{is}) distributions at various spanwise locations for the two Co-Flow Jet wings and baseline wing at aspect ratio 20 and at AoA of 5° are shown in Fig. 7. Fig. 7 indicates that the CFJ wings have higher loading than the baseline wing across the whole span due to the higher total lift coefficient. The inner 75% span of the CFJ and baseline wings have the similar loading. For the outer 25% span, the loading is gradually decreased due to the wing tip effect. The spikes on the Isentropic Mach number plot are due to the injection and suction slots. The CFJ greatly augments the circulation due to the increased flow velocity on the suction surface. Furthermore, the two CFJ wings have a significantly higher suction peak near the leading edge than the baseline wing. The higher suction peak Mach number increases the lift and reduces the pressure drag of the wing. The maximum M_{is} of the CFJ wing is about 0.27, an increase of roughly 8% over that of the baseline wing. Comparing the CFJ 1 wing with the CFJ 2 wing, a small difference is that a constant higher Mach number between the 60% and 80% chord, which is the result of enlarging the suction slot located at the 80% chord with the upstream surface curvature altered. This constant Mach number area on the airfoil suction surface makes a small contribution to the overall lift enhancement.

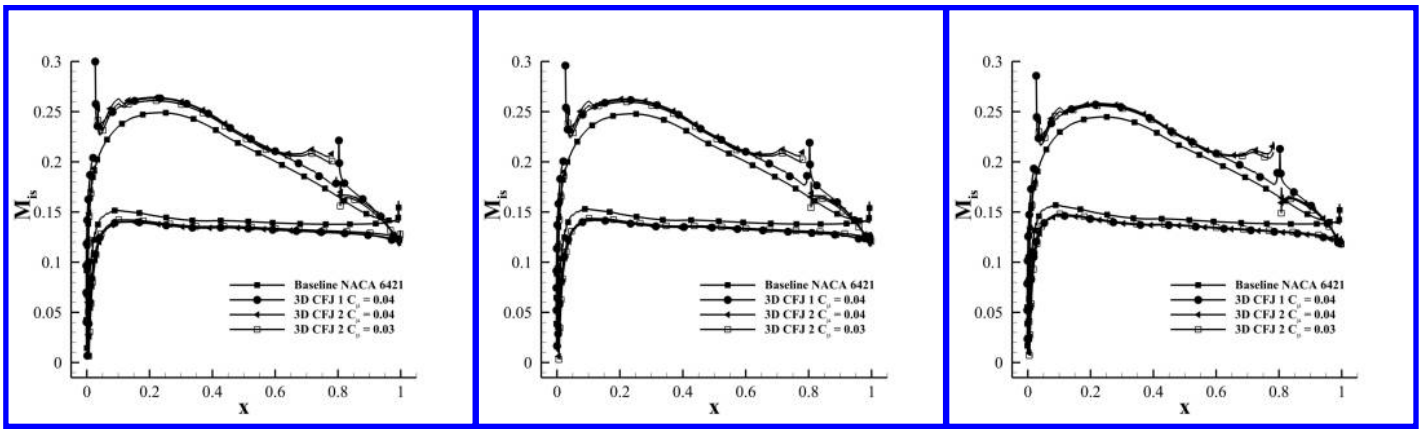

(a) M_{is} at 0% spanwise location (b) M_{is} at 50% spanwise location (c) M_{is} at 75% spanwise location

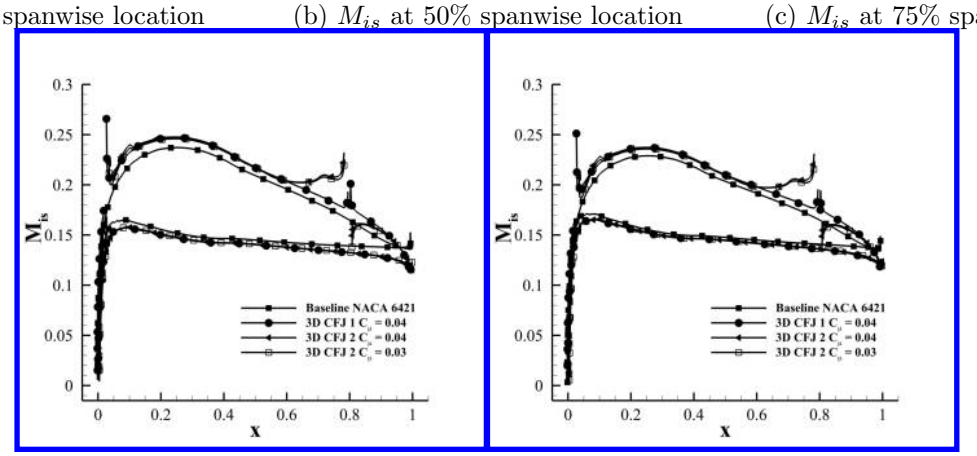

(d) M_{is} at 90% spanwise location (e) M_{is} at 95% spanwise location

Figure 7: Isentropic Mach number at various spanwise location for baseline wing, the CFJ 1 wing, the CFJ 2 wing at AR = 20 and AoA = 5°.

Figure. 8 is the Mach contours with streamlines at 0%, 50%, 75% and 95% spanwise location for the CFJ 1 wing, the CFJ 2 wing and the baseline wing at AR =20, AoA = 5°. As we can see on the suction surface of the wings, Co-Flow Jet wing gives a higher LE acceleration which is the source of the lift enhancement and pressure drag reduction. The baseline wing has a very small separation near the trailing edge due to the thick airfoil generating a fairly strong adverse pressure gradient. The CFJ wings do not have any flow separation.

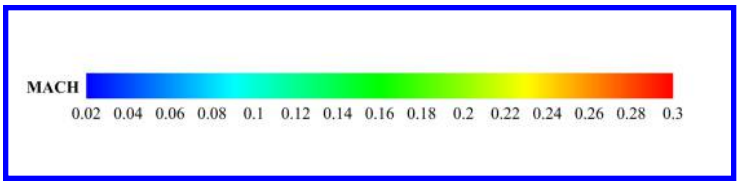

(a) Baseline Wing (b) CFJ 1 Wing at C_μ 0.04 (c) CFJ 2 Wing at C_μ 0.04 (d) CFJ 2 Wing at C_μ 0.03

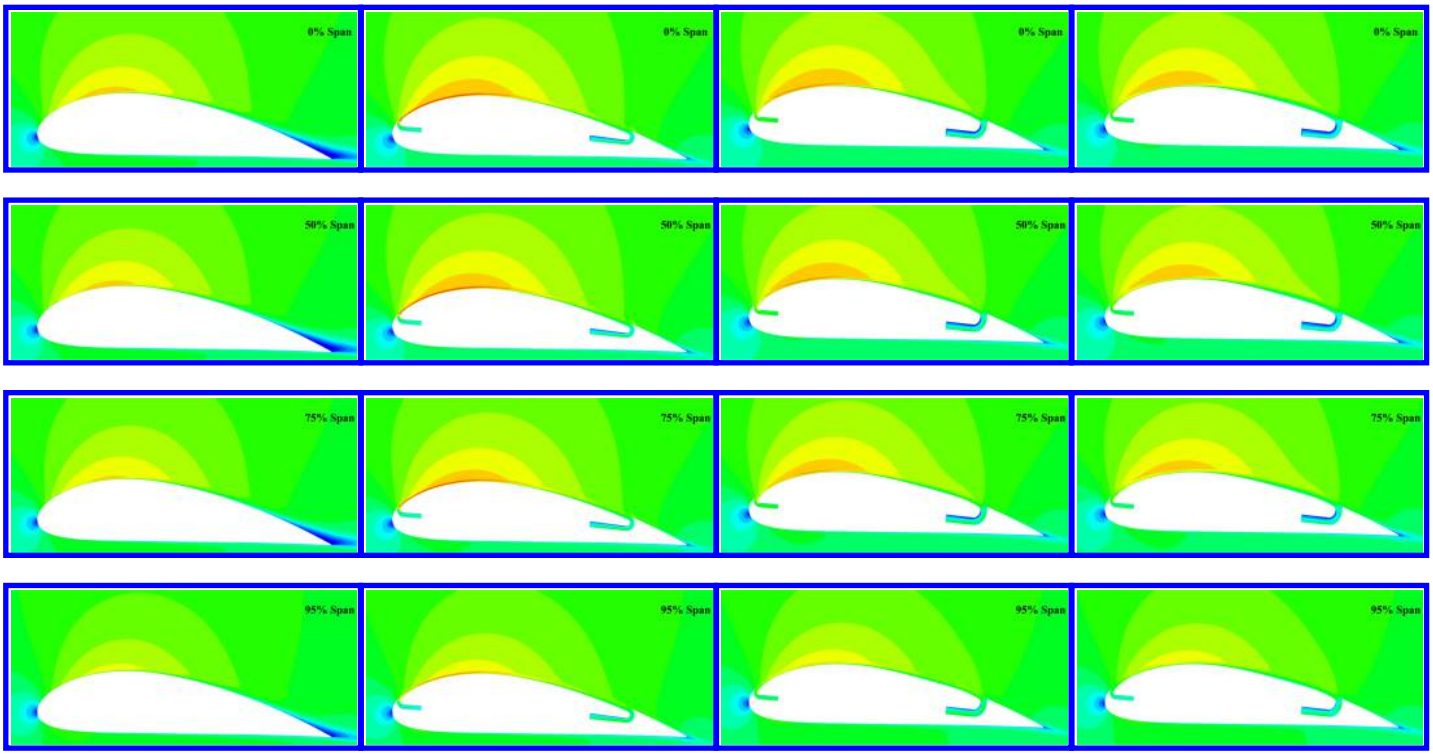

Figure 8: Mach contours with streamlines at 0%, 50%, 75% and 95% spanwise location for baseline wing, the CFJ 1 wing and the CFJ 2 wing at AR =20, AoA = 5° and $C_\mu = 0.04$.

Fig. 9 and Fig. 10 are the surface Isentropic Mach number distributions and the Mach contours at various spanwise location for the AR 5. The overall trends are very similar to the case of AR 20, but with smaller surface loading due to reduced lift coefficient.

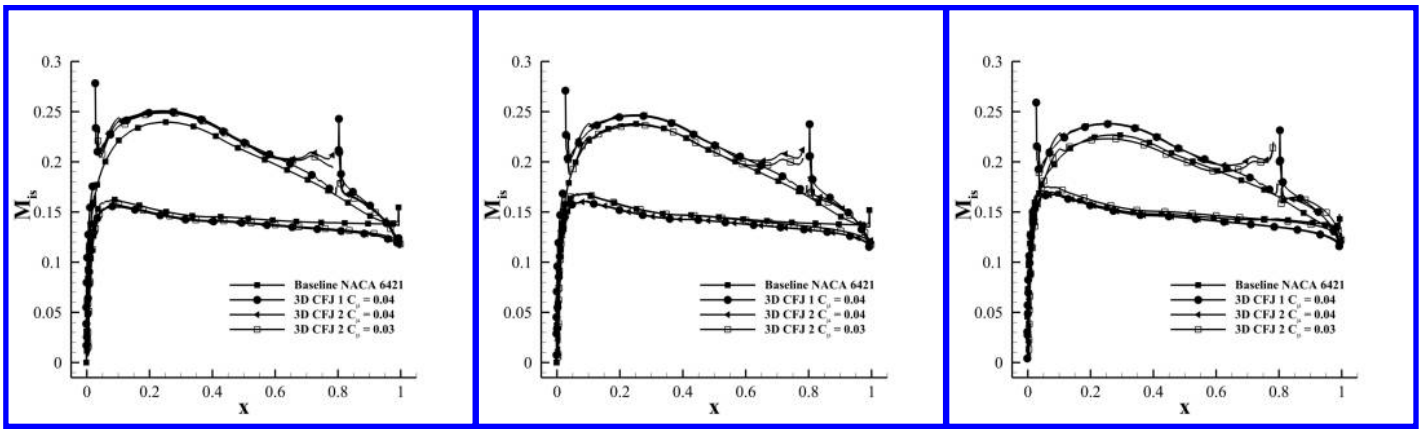

(a) M_{is} at 0% spanwise location (b) M_{is} at 50% spanwise location (c) M_{is} at 75% spanwise location

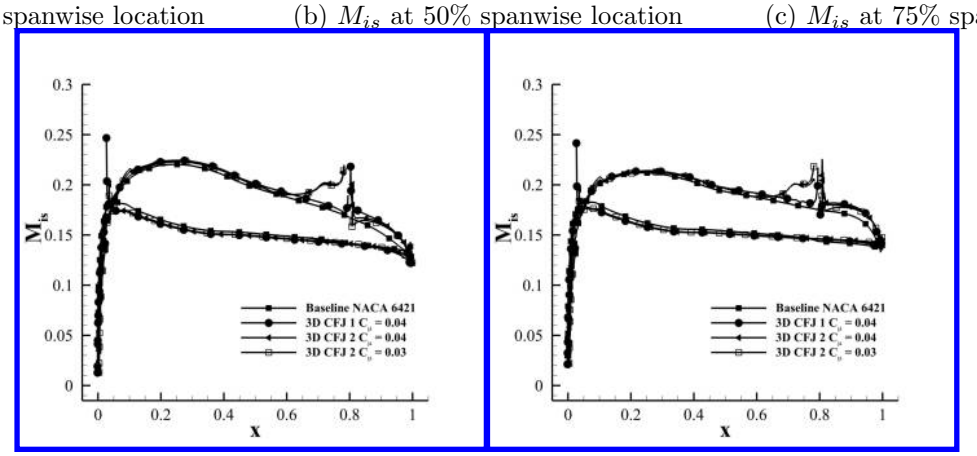

(d) M_{is} at 90% spanwise location (e) M_{is} at 95% spanwise location

Figure 9: Isentropic Mach number at various spanwise location for baseline wing, the CFJ 1 wing, and the CFJ 2 wing at AR = 5 and AoA = 5°

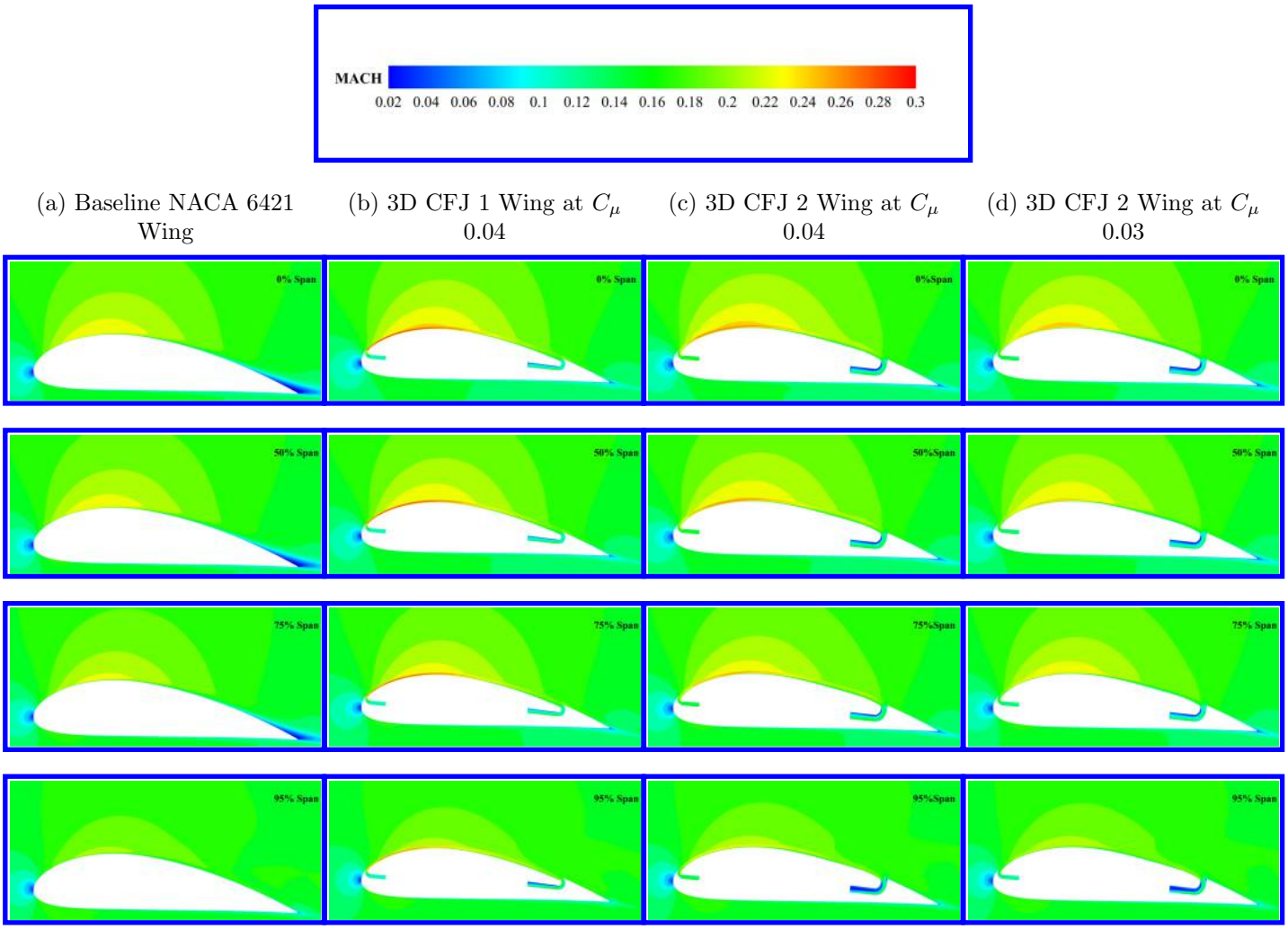

(a) Baseline NACA 6421 Wing | (b) 3D CFJ 1 Wing at C_μ 0.04 | (c) 3D CFJ 2 Wing at C_μ 0.04 | (d) 3D CFJ 2 Wing at C_μ 0.03

Figure 10: Mach contours with streamlines at 0%, 50%, 75% and 95% spanwise location for baseline wing, the CFJ 1 wing and the CFJ 2 wing at AR =5, AoA = 5° and $C_\mu = 0.04$.

Fig.11 shows the CFJ 2 wing surface static pressure contours with the streamlines showing tip vortex colored with the vorticity at AR 20, 10, and 5. They are plotted with the same scale for comparison.

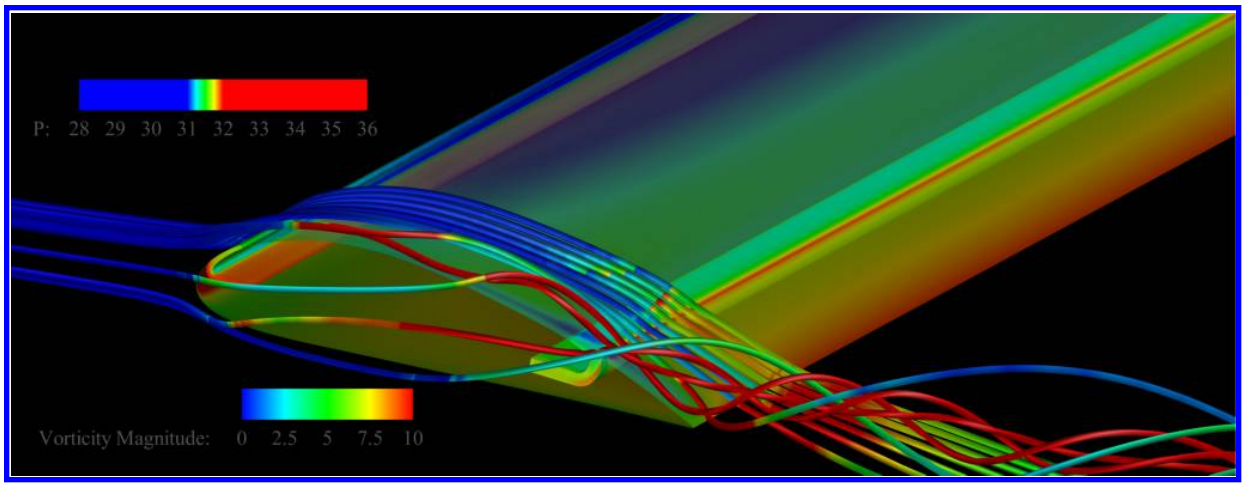

(a) 3D CFJ 2 Wing at AR 20 and C_μ 0.03

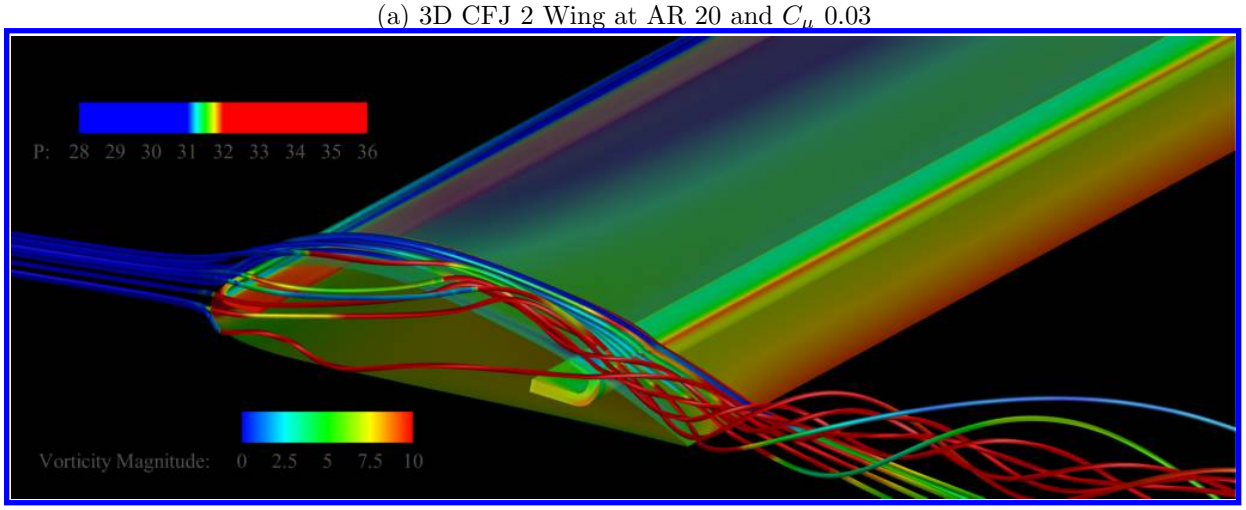

(b) 3D CFJ 2 Wing at AR 10 and C_μ 0.03

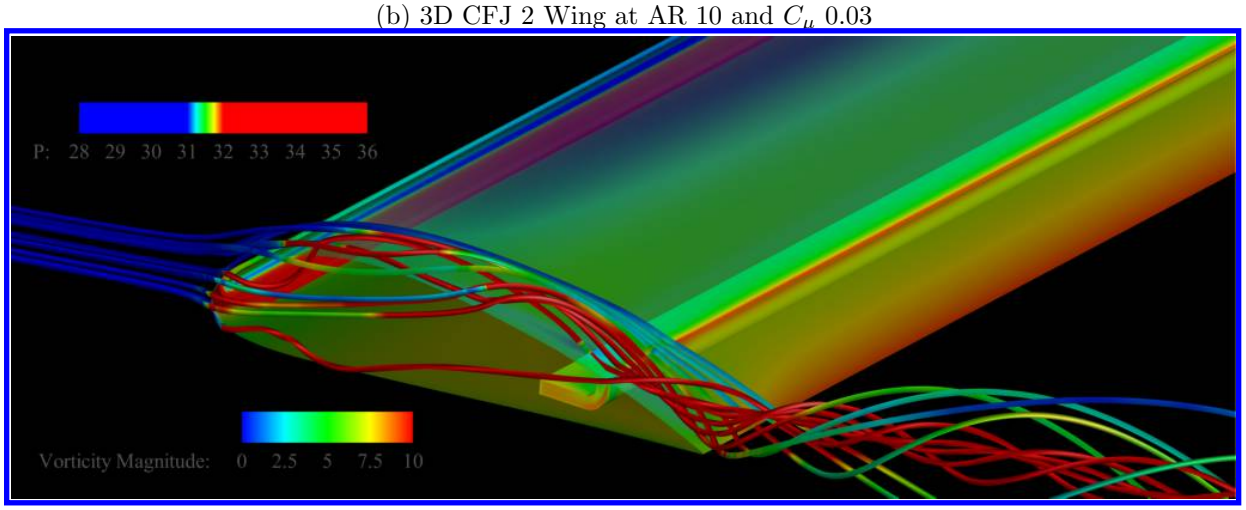

(c) 3D CFJ 2 Wing at AR 5 and C_μ 0.03

Figure 11: Tip vortex shown at pressure distribution and the tip vorticity magnitude plot of the CFJ 2 wing of aspect ratio 20, 10, 5 at AoA 5.

4 Mesh Independence Study

The mesh independence study is conducted with the mesh size doubled in ξ, η, ζ direction respectively once at a time. The mesh independence study is conducted at AoA of 5° only since the focus of this study is the cruise performance. Table 4, Table 5, and Table 6 give the coefficient of lift, drag, pitching moment, CFJ power, and required pumping total pressure ratio for 3D CFJ 2 wing at AR 20, 10 and 5 respectively. The variation of all results is within 1% and indicates that the solution is mesh size independent.

Table 4: Mesh independence study for the CFJ 1 wing at AoA = 5° and at aspect ratio 20.

Case	AoA	Grid size	C_L	C_D	C_M	P_c	P_r
Original	5°	$281 \times 81 \times 121$	1.183	0.0322	-0.1663	0.0085	1.0101
ξ	5°	$561 \times 81 \times 121$	1.180	0.0321	-0.1652	0.0083	1.0099
η	5°	$281 \times 161 \times 121$	1.164	0.0312	-0.1661	0.0083	1.0099
ζ	5°	$281 \times 81 \times 241$	1.185	0.0323	-0.1667	0.0085	1.0100

Table 5: Mesh independence study for the CFJ 1 wing at AoA = 5° and at aspect ratio 10.

Case	AoA	Grid size	C_L	C_D	C_M	P_c	P_r
Original	5°	$281 \times 81 \times 121$	1.068	0.0458	-0.1623	0.0096	1.0114
ξ	5°	$561 \times 81 \times 121$	1.065	0.0456	-0.1612	0.0093	1.0111
η	5°	$281 \times 161 \times 121$	1.051	0.0444	-0.1571	0.0095	1.0113
ζ	5°	$281 \times 81 \times 241$	1.069	0.0457	-0.1625	0.0096	1.0114

Table 6: Mesh independence study for the CFJ 1 wing at AoA = 5° and at aspect ratio 5.

Case	AoA	Grid size	C_L	C_D	C_M	P_c	P_r
Original	5°	$281 \times 81 \times 121$	0.897	0.0606	-0.1544	0.0110	1.0131
ξ	5°	$561 \times 81 \times 121$	0.896	0.0611	-0.1532	0.0103	1.0123
η	5°	$281 \times 161 \times 121$	0.870	0.0560	-0.1461	0.0110	1.0130
ζ	5°	$281 \times 81 \times 241$	0.899	0.0606	-0.1546	0.0109	1.0130

5 Conclusions

The study indicates that the induced drag coefficient of CFJ wings is increased with the decrease of aspect ratio. However, the Oswald efficiency is also increased with decreasing aspect ratio. The CFJ wings have higher Oswald efficiency than the baseline wings with the same aspect ratio becasue the lift enhancement effect outperforms the induced drag increase. In other words, the CFJ wing is less penalized even though the lift coefficient is higher than the baseline wing. The CFJ wing always has substantially higher ratio of C_L/C_D than the baseline wing since CFJ reduces the pressure drag significantly. For the corrected aerodynamic efficiency of $(C_L/C_D)_c$ that includes the CFJ power consumption, the CFJ 2 wing's result is slightly better than the baseline wing at aspect ratio of 20 and similar at aspect ratio of 10 and 5. However, attributed to the increased cruise lift coefficient, the productivity

efficiency of the CFJ 2 wing measured by $(C_L^2/C_D)_c$ is increased by 32.1% for the wing of AR 20, 19.4% for AR 10 and 5.6% for AR 5.

For the power consumption comparison, the CFJ 2 wings at all aspect ratios have substantially lower CFJ power coefficient benefited from the larger injection and suction slot size. For the same momentum coefficient, the CFJ 2 wings with larger slot size have lower injection velocity, lower total pressure ratio between the injection and suction slot, and larger mass flow rate. The CFJ power coefficient is determined linearly by the mass flow rate, but exponentially by the total pressure ratio. Hence a decrease of the total pressure ratio has the major impact to reduce the CFJ power consumption. As a result, the productivity efficiency of the CFJ 2 wing is increased by 12.9%, 9.8% and 8.7% for AR 20, 10 and 5 respectively compared with the CFJ 1 wing.

In conclusion, the CFJ wing is much more efficient than the baseline wing at either high or low aspect ratio. Furthermore, the CFJ power consumption can be substantially reduced by using large slot size with reduced injection jet velocity and jet total pressure ratio. This is particularly important for the same CFJ airfoil with fixed geometry to be used for whole flight envelop from takeoff to cruise and landing.

6 Acknowledgment

The simulations are conducted on Pegasus supercomputing system at the Center for Computational Sciences at the University of Miami.

References

[1] G.-C. Zha and D. C. Paxton, "A Novel Flow Control Method for Airfoil Performance Enhancement Using Co-Flow Jet." *Applications of Circulation Control Technologies*, Chapter 10, p. 293-314, Vol. 214, Progress in Astronautics and Aeronautics, AIAA Book Series, Editors: Joslin, R. D. and Jones, G.S., 2006.

[2] G.-C. Zha, W. Gao, and C. Paxton, "Jet Effects on Co-Flow Jet Airfoil Performance," *AIAA Journal, No. 6,*, vol. 45, pp. 1222–1231, 2007.

[3] G.-C. Zha, C. Paxton, A. Conley, A. Wells, and B. Carroll, "Effect of Injection Slot Size on High Performance Co-Flow Jet Airfoil," *AIAA Journal of Aircraft*, vol. 43, 2006.

[4] G.-C. Zha, B. Carroll, C. Paxton, A. Conley, and A. Wells, "High Performance Airfoil with Co-Flow Jet Flow Control," *AIAA Journal*, vol. 45, 2007.

[5] Wang, B.-Y. and Haddoukessouni, B. and Levy, J. and Zha, G.-C., "Numerical Investigations of Injection Slot Size Effect on the Performance of Co-Flow Jet Airfoil," *Journal of Aircraft*, vol. Vol. 45, No. 6,, pp. pp.2084–2091, 2008.

[6] B. P. E. Dano, D. Kirk, and G.-C. Zha, "Experimental Investigation of Jet Mixing Mechanism of Co- Flow Jet Airfoil." AIAA-2010-4421, 5th AIAA Flow Control Conference, Chicago, IL, 28 Jun - 1 Jul 2010.

[7] B. P. E. Dano, G.-C. Zha, and M. Castillo, "Experimental Study of Co-Flow Jet Airfoil Performance Enhancement Using Micro Discreet Jets." AIAA Paper 2011-0941, 49th AIAA Aerospace Sciences Meeting, Orlando, FL, 4-7 January 2011.

[8] A. Lefebvre, B. Dano, W. Bartow, M. Fronzo, and G. Zha, "Performance and energy expenditure of coflow jet airfoil with variation of mach number," *Journal of Aircraft*, vol. 53, no. 6, pp. 1757–1767, 2016.

[9] A. Lefebvre, G-C. Zha, "Numerical Simulation of Pitching Airfoil Performance Enhancement Using Co-Flow Jet Flow Control," *AIAA paper 2013-2517*, June 2013.

[10] A. Lefebvre, G-C. Zha, "Cow-Flow Jet Airfoil Trade Study Part I : Energy Consumption and Aerodynamic Performance," *32nd AIAA Applied Aerodynamics Conference, AIAA AVIATION Forum, AIAA 2014-2682*, June 2014.

[11] A. Lefebvre, G-C. Zha, "Cow-Flow Jet Airfoil Trade Study Part II : Moment and Drag," *32nd AIAA Applied Aerodynamics Conference, AIAA AVIATION Forum, AIAA 2014-2683*, June 2014.

[12] Lefebvre, A. and Zha, G.-C., "Trade Study of 3D Co-Flow Jet Wing for Cruise Performance." AIAA Paper 2016-0570, AIAA SCITECH2016, AIAA Aerospace Science Meeting, San Diego, CA, 4-8 January 2016.

[13] Gecheng Zha, Yunchao Yang, Yan Ren, Brendan McBreen, "Super-Lift and Thrusting Airfoil of Coflow Jet Actuated by Micro-Compressors." AIAA Paper-2018-3061, AIAA AVIATION Forum 2018, 2018 Flow Control Conference, Atlanta, Georgia, June 25-29, 2018.

[14] Lefebvre, A. and Zha, G.-C. , "Design of High Wing Loading Compact Electric Airplane Utilizing Co-Flow Jet Flow Control." AIAA Paper 2015-0772, AIAA SciTech2015: 53nd Aerospace Sciences Meeting, Kissimmee, FL, 5-9 Jan 2015.

[15] Yunchao Yang and Gecheng Zha, ""Numerical Investigation of Performance Improvement of the Co-Flow Jet Electric Airplane." AIAA Paper-2018-4208, AIAA AVIATION Forum 2018, 2018 Applied Aerodynamics Conference, Atlanta, Georgia, June 25-29, 2018.

[16] Yunchao Yang and Gecheng Zha, "Super-Lift Coefficient of Active Flow Control Airfoil: What is the Limit?." AIAA Paper 2017-1693, AIAA SCITECH2017, 55th AIAA Aerospace Science Meeting, Grapevine, January 9-13 2017.

[17] Lefebvre, A. and Dano, B. and Bartow, W. and Di Franzo, M. and Zha, G.-C., "Performance Enhancement and Energy Expenditure of Co-Flow Jet Airfoil with Variation of Mach Number." AIAA Paper 2013-0490, AIAA Journal of Aircraft, DOI: 10.2514/1.C033113, 2016.

[18] P. R. Spalart and S. R. Allmaras, "A one-equation turbulence model for aerodynamic flows," in *30th Aerospace Sciences Meeting and Exhibit, Aerospace Sciences Meetings, Reno, NV, USA, AIAA Paper 92-0439*, 1992.

[19] Y.-Q. Shen and G.-C. Zha, "Large Eddy Simulation Using a New Set of Sixth Order Schemes for Compressible Viscous Terms ," *Journal of Computational Physics*, vol. 229, pp. 8296–8312, 2010.

[20] Zha, G.C., Shen, Y.Q. and Wang, B.Y., "An improved low diffusion E-CUSP upwind scheme ," *Journal of Computer and Fluids*, vol. 48, pp. 214–220, Sep. 2011.

[21] Y.-Q. Shen and G.-Z. Zha , "Generalized finite compact difference scheme for shock/complex flowfield interaction," *Journal of Computational Physics*, vol. doi:10.1016/j.jcp.2011.01.039, 2011.

[22] Shen, Y.-Q. and Zha, G.-C. and Wang, B.-Y., " Improvement of Stability and Accuracy of Implicit WENO Scheme," *AIAA Journal*, vol. 47, No. 2, pp. 331–344, 2009.

[23] Shen, Y.-Q. and Zha, G.-C. and Chen, X.-Y., " High Order Conservative Differencing for Viscous Terms and the Application to Vortex-Induced Vibration Flows," *Journal of Computational Physics*, vol. 228(2), pp. 8283–8300, 2009.

[24] Shen, Y.-Q. and Zha, G.-C. , " Improvement of the WENO Scheme Smoothness Estimator," *International Journal for Numerical Methods in Fluids*, vol. DOI:10.1002/fld.2186, 2009.

[25] G.-C. Zha and E. Bilgen, "Numerical Study of Three-Dimensional Transonic Flows Using Unfactored Upwind-Relaxation Sweeping Algorithm," *Journal of Computational Physics*, vol. 125, pp. 425–433, 1996.

[26] B.-Y. Wang and G.-C. Zha, "A General Sub-Domain Boundary Mapping Procedure For Structured Grid CFD Parallel Computation," *AIAA Journal of Aerospace Computing, Information, and Communication*, vol. 5, No.11, pp. 2084–2091, 2008.

[27] Y.-Q. Shen, G.-C. Zha, and B.-Y. Wang, "Improvement of Stability and Accuracy of Implicit WENO Scheme ," *AIAA Journal*, vol. 47, pp. 331–344, 2009.